ISSN No: 2348-4845
International Journal & Magazine of Engineering, Technology, Management and Research
A Peer Reviewed Open Access International Journal

LCC & LLC Resonant Converter For High-Power, Low-Voltage, High-Current Power Applications

B.Anurag
M.Tech (Power Electronics),
Dept of EEE,
St.Martin's Engineering College.

V.Sunil Kumar, M.E (EPS)
Associate Professor,
Dept of EEE,
St.Martin's Engineering College.

ABSTRACT:
LCC thunderous converter with inductive channel working in spasmodic current mode (DCM) can accomplish zero-current exchanging (ZCS) for both the force switches and rectifier diodes. In this way, it is appropriate for high-control, low-voltage, high-current force supplies. The DCM LCC resounding converter with inductive channel may work in various working modes when info voltage or burden changes, which challenges the outline. This paper infers a mode limit map, from which the working method of the converter can be effectively decided. In light of the mode limit outline, summed up ideal configuration technique is proposed and an arrangement of ideal and standardized converter parameters is resolved, which can be effectively changed over into genuine parameters as indicated by the converter detail. Three 5 kW models with various converter parameters are created and tried in the lab, and the exploratory results demonstrate that with the arrangement of ideal parameters, the converter can accomplish the most astounding proficiency over the whole info voltage and burden range.

Index Terms:
Discontinuous current mode (DCM), *LCC* resonant converter, mode boundary map, optimal design, zero-current switching (ZCS**).**

I. INTRODUCTION:

High-control, low-voltage, high-current force supplies are broadly utilized as a part of electroplating [1], electrolyzing [2], welding [3] and excitation for superconducting magnet [4], and so on.

In these force supplies, IGBTs are usually utilized as the force switches. It is liked to accomplish zero-current exchanging (ZCS) for IGBTs to diminish the turn-off misfortunes came about by the present tail [5]. Full converters are great possibility for accomplishing ZCS. Arrangement full converter (SRC) [6] and parallel thunderous converter (PRC) [7] are two essential resounding converters. SRC offers high productivity at light load, yet it has an extensive variety of exchanging recurrence and its yield voltage can't be controlled at a heap [8]. PRC has a restricted scope of exchanging recurrence, and its yield voltage can be controlled at no heap; be that as it may, the effectiveness at light load is generally low [8]. Keeping in mind the end goal to beat the weaknesses of SRC and PRC, different other full converters with more than two thunderous parts have been proposed [9], [10].

Among them, LLC full converter [11], [12] and LCC thunderous converter [13]–[24] are the most well known converters. The yield channel of a thunderous converter can be either a capacitive channel or an inductive channel [9], [10]. For the LLC full converter, the yield channel ought to be the capacitive one. For the LCC resounding converter, both the capacitive channel [13]–[19] and inductive channel [20]–[24] can be embraced. In high-control, low-voltage, high-current force supplies, the inductive channel is alluring since the present swell in the yield channel capacitor is moderately littler contrasted with that in the capacitive channel. There-fore, LCC thunderous converter with inductive channel is appealing for these applications. The LCC thunderous converter with inductive channel can work in constant current mode (CCM) [20]–[22]

ISSN No: 2348-4845
International Journal & Magazine of Engineering, Technology, Management and Research
A Peer Reviewed Open Access International Journal

or intermittent current mode (DCM) [23], [24]. In CCM, if the LCC resounding converter with inductive channel works above reverberation, the force switches can accomplish zero-voltage exchanging (ZVS) [20], [21]; on the off chance that it works beneath reverberation, the force switches can accomplish ZCS turn-off, however hard turn-on [22]. In DCM, both the ZCS turn-on and turn-off can be accomplished, prompting low exchanging misfortunes [23], [24]. In this way, letting the LCC thunderous converter with inductive channel to work in DCM is a superior decision for high-control, low-voltage, high-current applications.

The framework of LCC reverberating converter has been extensively inspected [13]–[24], and the DCM LCC full converter with inductive channel has been based on in [23] and [24]. The DCM LCC deafening converter with inductive direct can work in various working modes, and the working mode may change with the assortments of information voltage and weight, which challenges the layout of the converter parameters. In [23] and [24], two distinctive working modes are considered for configuration, separately, and in this way, the converter has not been enhanced with varieties of the info voltage and burden. Besides, outlines depend on the particular determinations of the converters.

For different details, the converter ought to be overhauled. To tackle these issues, this paper proposes the idea of the mode limit map for the DCM LCC full converter with inductive channel, from which the working method of the converter can be effortlessly decided. In light of the mode limit delineate, summed up ideal outline system with the varieties of information voltage and burden is proposed and an arrangement of standardized converter parameters is resolved, which can be effectively changed over into genuine converter parameters, regardless of what the converter particular is. With this arrangement of parameters, the converter can accomplish a high effectiveness over the whole information voltage and burden ranges.

This paper is sorted out as takes after. In Section II, the conceivable working methods of the DCM LCC resounding converter with inductive channel are quickly looked into. In Section III, the mode limit guide is determined. In Section IV, the enduring state qualities of the converter are given. In Section V, an arrangement of ideal and standardized converter parameters is resolved in view of the mode limit map. In Section VI, three 50 V/100 A proto-sorts are manufactured and tried. One model is planned with the proposed set of ideal parameters; the other two proto-sorts are utilized for examinations. In these two models, one is outlined with the arrangement of parameters from [24], and the other is composed with the parameters so it goes about as a DCM PRC. The test comes about check that the model with the proposed set of parameters accomplishes a higher effectiveness than the other two models over the whole information voltage and burden range. At long last, Section VII finishes up this paper.

II. REVIEW OF OPERATING MODES OF DCM LCC RESONANT CONVERTER WITH INDUCTIVE FILTER

Fig. 1 demonstrates the primary circuit of the LCC resounding converter with inductive channel. The parallel full capacitor Cp is purposefully set on the auxiliary side of the transformer to make utilization of the spillage inductor of the transformer as a part of the thunderous inductor. The inductor Lr speaks to the aggregate of the resounding inductor and the spillage inductor of the transformer. Lf and Cf form the inductive channel. The converter is operated in DCM by gating the switches Q1−Q4 with an altered on-time and variable recurrence to manage the yield voltage. Before investigation, it is accepted that every one of the segments are perfect and Lf is sufficiently vast to be viewed as a present source with the estimation of yield current Io. Because of the symmetrical operation, just the half cycle when Q1 and Q4 are leading is investigated here. Fig. 2 demonstrates all the conceivable identical circuits during diverse working interims down the middle cycle, where the circuit shaped by Lf , Cf , and RL d is improved to the present

ISSN No: 2348-4845
International Journal & Magazine of Engineering, Technology, Management and Research
A Peer Reviewed Open Access International Journal

source Io and the parallel thunderous capacitor Cp is reflected to the essential side of the transformer, meant by Cp.

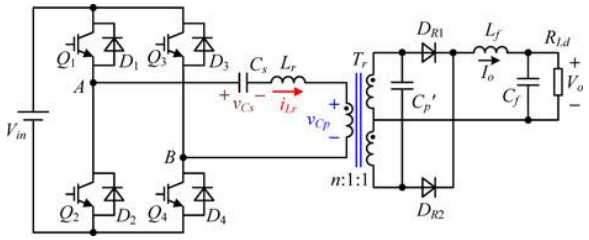

Fig.1.Main circuit of the *LCC* resonant converter with inductive filter.

Interval 0 [Prior to 0]:

i_{Lr}=0 and the load current$I_o$freewheels through D_{R1} and D_{R2} . Therefore, v_{Cp} = 0 and $v_{C\,s}$ has an initial value.

Interval 1 [t_0, t_1]: Att$_0$,Q_1, and$Q_4$are turned on with ZCS,andV_{in} is applied on the resonant tank. Consequently, L_r and $C_s$start to resonate, andi_{Lr}increases from zero. Asi_{Lr}<I_o/n, $D_{R1}$and D_{R2}still keep conducting andv_{Cp}=0.

Interval 2 [After t_1]:

Att$_1$,i_{Lr}increasestoI$_o$/n.D_{R2}turnsoff naturally, and I_o flows through D_{R1} . After t_1,i_{Lr}>I_o /n. Hence, C_p is charged and v_{Cp} increases from zero. L_r ,C_s , and $C_p$start to resonate.Over the span of reverberation, iLr will cross zero twice: the first run through is that iLr crosses zero from the positive bearing, indicated by ti+; and the second time is that iLr crosses zero from the negative course, meant by ti−. vC p will cross zero once from the positive course, meant by tv+. tv+ could be later than ti−, inside [ti+ , ti−], or sooner than ti+ , and this will prompt three conceivable working modes, which are named as Mode 1, Mode 2, and Mode 3, separately. The key working waveforms of these three working modes are appeared in Fig. 3. In these working modes, Q1 and Q4 are killed with ZCS when iLr decreases to negative and moves through D1 and D4 during [ti+,ti−].At the point when both iLr and v Cp return to zero, the converter will come back to Interval 0. The nitty gritty conditions of Mode 1 and Mode 2 can be found from [23] and [24], separately. The standardized types of the conditions of all these three working modes are determined in Appendix A.

The physical amounts in these conditions are standardized as for the base amounts characterized in Table I. Unfaltering state arrangements of the converter can be gotten from these conditions.

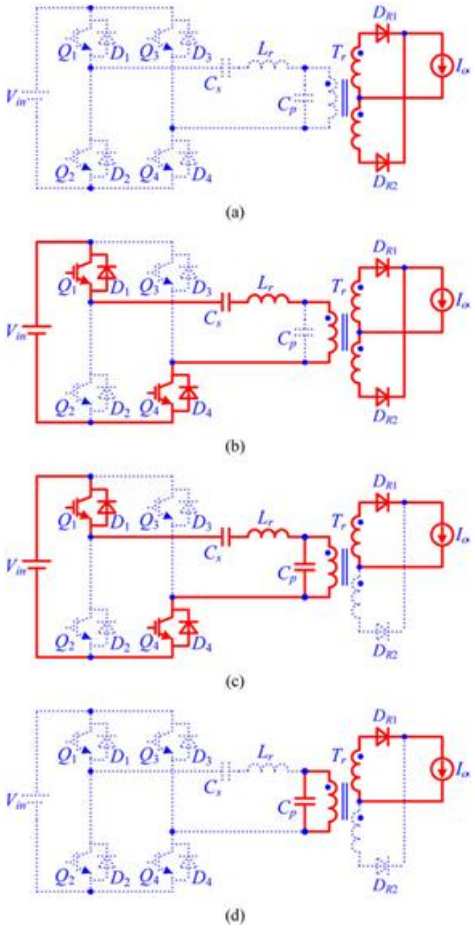

Fig. 2. Possible operating intervals in half cycle.(a) Interval 0. (b) Interval 1.(c) Interval 2. (d) Interval 3

TABLE I: DEFINITION OF BASE QUANTITIES

Voltage	Impedance	Current	Time	Frequency
V_{in}	Z_r	V_{in}/Z_r	$1/\omega_r$	f_r

ISSN No: 2348-4845
International Journal & Magazine of Engineering, Technology, Management and Research
A Peer Reviewed Open Access International Journal

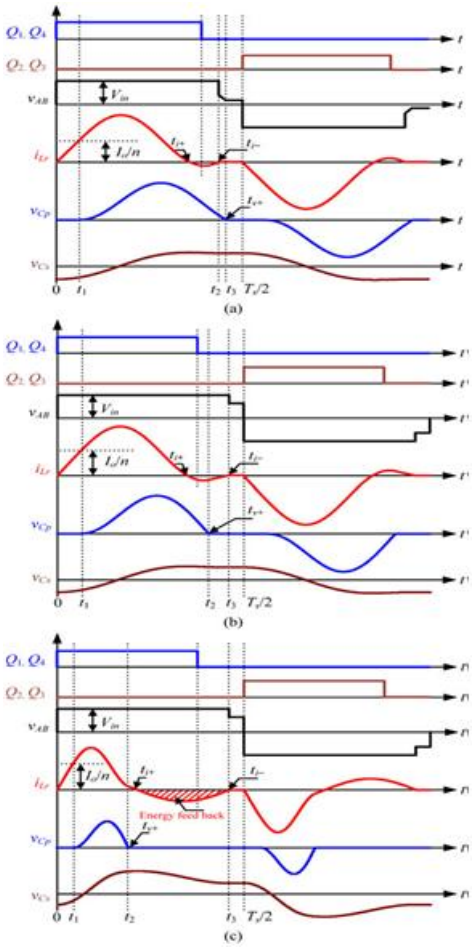

Fig. 3. Key operating waveforms. (a) Mode 1. (b) Mode 2. (c) Mode 3.

III. DERIVATION OF THE MODE BOUNDARY MAP

A. Boundary Curve between Mode 1 and Non-ZCS Area:

As seen in Fig. 3(a), L_rC_s and C_p resonate after t_1 in Mode 1. In order to achieve ZCS turn-off for the power switches, i_{Lr} should cross zero. So, according to (A8), we have

$$\frac{I_{oN}}{1+\lambda} \le \sqrt{\left(\frac{\lambda I_{oN}}{1+\lambda}\right)^2 + (1-V_{C_sN1})^2}. \quad (1)$$

According to (1), the boundary condition between Mode 1 and non-ZCS area is

$$\frac{I_{oN}}{1+\lambda} = \sqrt{\left(\frac{\lambda I_{oN}}{1+\lambda}\right)^2 + (1-V_{C_sN1})^2}. \quad (2)$$

Combining and solving (2), (A5), (A9), (A11), and (A16) can obtain the equation of the boundary curve of Mode 1 and non-ZCS area as

$$I_{oN} = \frac{2}{\frac{1+(1-\lambda)^{3/2}}{\sqrt{1+\lambda}} - \frac{\lambda(1.5\pi - \arcsin\lambda - \lambda\sqrt{1-\lambda^2})}{(1+\lambda)^2}} \quad (3)$$

where $I_{o\ N} = I_oZ_r/(nV_{in})$, $\lambda = C_p/C_s$. The detailed derivation of (3) is shown in Appendix B. According to (3), Curve 1, which is the boundary curve between Mode 1 and non-ZCS area, is drawn in Fig. 4.

B. Boundary Curve Between Mode 1 and Mode 2

$t_{v+}=t_{i-}$is the boundary condition between Mode 1 andMode 2. This implies $V_{C\ pN\ 2} = 0$ in Mode 1. Likewise, combining and solving $V_{C\ pN\ 2} = 0$, (A5), (A9)–(A11), and (A16), the boundary curve equation between Mode 1 and Mode 2 can be derived as

$$\begin{cases} \tan\left(\frac{\alpha_{12}}{2}\right) + \frac{\lambda\alpha_{12}}{1-\lambda} = 0 \\ I_{oN} = \sqrt{\left(\frac{1-\lambda^2-\lambda^2\alpha_{12}^2}{\lambda\alpha_{12}}\right)^2 + 4(1+\lambda)} - \frac{1-\lambda^2-\lambda^2\alpha_{12}^2}{\lambda\alpha_{12}}. \end{cases} \quad (4)$$

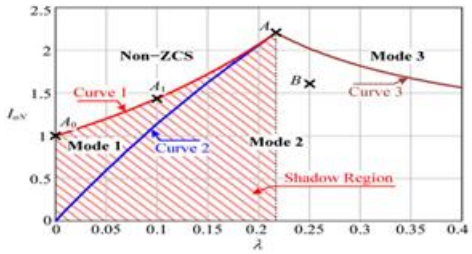

Fig. 4.Mode boundary map of DCM LCC resonant converter with inductive filter.

According to (4), Curve 2, which is the boundary curve be-tween Mode 1 and Mode 2, is drawn in Fig. 4.

C. Boundary Curve Between Mode 2 and Mode 3

$t_{v+}=t_{i+}$is the boundary condition between Mode 2 andMode 3. This implies $I_{L\ rN\ 2} = 0$ in Mode 2. Likewise, solving $I_{L\ rN\ 2}=0$, (A5), (A17)–(A19), (A23), (A24), and (A25), theequation of the boundary curve between Mode 2 and Mode 3 can be derived as

ISSN No: 2348-4845
International Journal & Magazine of Engineering, Technology, Management and Research
A Peer Reviewed Open Access International Journal

$$\begin{cases} \tan(\alpha_{12}/2)+\lambda\alpha_{12}/(1-\lambda)=0 \\ I_{oN}=\sqrt{\left(\dfrac{1-\lambda^2-\lambda^2\alpha_{12}^2}{\lambda\alpha_{12}}\right)^2+4(1+\lambda)}+\dfrac{1-\lambda^2-\lambda^2\alpha_{12}^2}{\lambda\alpha_{12}} \end{cases} \quad (5)$$

According to (5), Curve 3, which is the boundary curve between Mode 2 and Mode 3, is drawn in Fig. 4. Since Curve 1 is the boundary curve between Mode 1 and non-ZCS area, it has $t_{i+} = t_{i-}$ on Curve 1. Likewise, on Curve 2, $t_{v+}=t_{i-}$. Therefore, at the intersection pointAof Curve 1and Curve 2, $t_{v+} = t_{i+}$, which is the condition of Curve 3. So Curve 3 also crosses point A. That means Curve 1, Curve 2, and Curve 3 intersect at the point A. By solving (3) and (4), we have $\lambda = 0.217, I_{oN}= 2.209$at pointA.

IV. STEADY-STATE CHARACTERISTICS OF THE CONVERTER:

In this section, the steady-state characteristics of the converter include voltage gain and component stresses will be analyzed to facilitate the optimal design.

A. Voltage Gain:

The voltage gain of the converter is defined as $V_{oN} = nV_o /V_{in}$. As seen in Fig. 1,V_{oN}equals to the average valueofv_{CpN} during $[t_0,T_s/2]$. Therefore, referring to Fig. 3, V_{oN} can be expressed as

$$V_{oN} = \frac{f_{sN}}{\pi}\int_{\alpha_1}^{\alpha_3} v_{C_pN}(\alpha)d\alpha \quad (6)$$

Where the expression of v_{CpN} (α) is (A7) when $\alpha_1\leq\alpha\leq\alpha_2$; and when $\alpha_2\leq\alpha\leq\alpha_3$, the expression of v_{CpN} (α) is (A13) for Mode 1, and v_{CpN} (α) = 0 for Mode 2 and Mode3. According to Appendix C, in Mode 1 and Mode 2, the approximate expression of V_{oN} can be obtained as

$$V_{oN} \approx \frac{2f_{sN}}{1+\lambda}. \quad (7)$$

In DCM, the maximum switching frequency is about the half of the resonant frequency f_r , which indicates the maximum $f_{sN}$is about 0.5. Substituting f_{sN}= 0.5into (7) gives that the maximum V_{oN} is about $1/(1 + \lambda)$. That means the voltage gain $V_{oN}$is always smaller than 1. It can also be known from (7) that when switching frequency and input voltage are constant, the output voltage will be constant and is independent of the load.

B. Component Stresses:

Referring to Fig. 3, the rms value of $i_{LrN}$is expressed as

$$I_{L_rN\_rms} = \sqrt{\frac{f_{sN}}{\pi}\int_0^{\alpha_3} i_{L_rN}^2(\alpha)d\alpha} \quad (8)$$

Where the expressions of i_{LrN} (α) are (A3) and (A8) when $0 \leq\alpha \leq \alpha_1$and $\alpha_1\leq \alpha \leq \alpha_2$respectively; and when $\alpha_2 \leq \alpha \leq\alpha_3$,$i_{LrN}(\alpha)$ is zero for Mode 1, and$i_{LrN}(\alpha)$ is expressed as(A22) for Mode 2 and Mode 3. As seen in Fig. 3, i_{LrN}reaches its peak value $I_{LrN\ pk}$ during$[t_1, t_2]$. From (A8), we have

$$I_{L_rN\_pk} = \frac{I_{oN}}{1+\lambda} + \sqrt{\left(\frac{\lambda I_{oN}}{1+\lambda}\right)^2 + (1-V_{C_sN1})^2}. \quad (9)$$

Again, as seen in Fig. 3, v_{CpN}reaches its peak value when$i_{Lr}=I_o/n$during$[t_1, t_2]$. From (A7) and (A8), we have

$$V_{C_pN\_pk} = \frac{2}{1+\lambda}\left[1 - V_{C_sN1} - \frac{\lambda I_{oN}}{1+\lambda}\arctan\frac{(1+\lambda)(1-V_{C_sN1})}{\lambda I_{oN}}\right]. \quad (10)$$

V. OPTIMAL DESIGN OF CONVERTER PARAMETERS BASED ON THE MODE BOUNDARY MAP:

In this section, a generalized optimal design will be implemented based on the mode boundary map to achieve a high efficiency over the entire input voltage and load range. As the design is based on normalized values, it is not necessary to know the specific values of the converter specification, and only the symbols of the specification are listed below:

1) Input voltage: $V_{in\ min}$ –$V_{in\ max}$;
2) Output voltage: V_o ;
3) Output current at full load: I_{omax} ;
4) Maximum switching frequency: f_{smax} .

As seen from (7), V_{oN} is proportional to f_{sN} and is independent of I_{oN}. That means the switching frequency doesn't vary with load and the variation range of switching frequency is proportional to the

ISSN No: 2348-4845
International Journal & Magazine of Engineering, Technology, Management and Research
A Peer Reviewed Open Access International Journal

variation range of input voltage. Therefore, the range of switching frequency cannot be reduced and when the maximum switching frequency f_{smax} is given, the minimum switching frequency is determined by the range of input voltage. In order to improve the converter efficiency, we should reduce the switching losses and conduction losses. Since the power switches can realize ZCS, the switching losses are quite small and can be ignored compared with conduction losses. Therefore, in order to improve the converter efficiency, we should mainly reduce the conduction losses, which mean the circulating current of the resonant tank should be reduced. Since the circulating current of the resonant tank will be reduced with the reduction of the energy that is fed back to the input voltage by the resonant tank. So the optimization goal is to achieve the lowest energy that is fed back to the input voltage by the resonant tank.

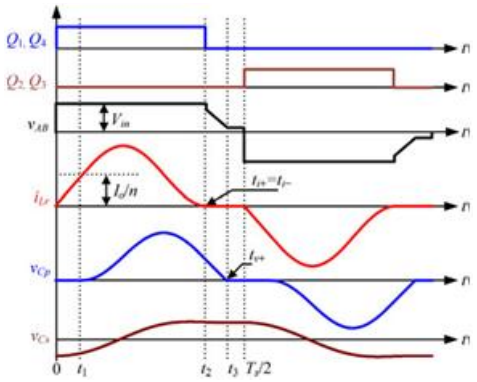

Fig. 5. Key operating waveforms on the boundary of Mode 1 and non-ZCSarea (Curve 1 in Fig. 4)

A. Determine the Optimal Parameters Based on the Mode Boundary Map

For a generalized design, four normalized parameters, includingλ, I_{oN} ,f_{sN} and V_{oN} are needed to be determined. First, λ and I_{oN} will be determined based on the mode boundary map.

1) Determine λ and I_{oN} Based on the Mode Boundary Map:

According to Fig. 3, in Mode 1, Mode 2, or Mode 3, at the point when iLr<0 during[t0,Ts/2], there is vitality encouraged back to the inputvoltage.

Clearly, the vitality that is encouraged back in Mode 3 is bigger than that in Mode 1 and Mode 2, which will bring about a low effectiveness. With a specific end goal to accomplish a high effectiveness, the vitality that is bolstered back to the information voltage ought to be decreased as little as would be prudent. On the limit of Mode 1 and non-ZCS territory, which is spoken to by Curve 1 in Fig. 4, the vitality that is sustained back is zero as appeared in Fig. 5, which infers that the converter will accomplish the most noteworthy proficiency when λ and IoN are composed on Curve 1.

Since IoN = IoZr/(nVin), IoN will reduction (or increment) with the lessening (or increment) of the heap current Io or the expansion (or diminishing) of the info voltage Vin . So from Fig. 4, if λ andIoNare outlined on Curve 1 under discretionary info voltageand load current conditions, when the information voltage diminish or the heap current increment, IoN will increment and in this way theconverter will go into the non-ZCS area, which will bring about the loss of ZCS and along these lines a decreased effectiveness. In this way, λ and IoN ought to be composed on Curve 1 under the state of least info voltage and full load current.

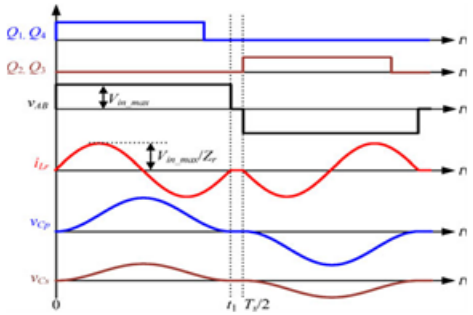

Fig. 6. Key operating waveforms at maximum input voltage and no load.

By planning λ and IoN on Curve 1 under the state of least info voltage and full load current, the resounding tank does not bolster vitality back to the information. At the point when the info voltage increments or burden current abatements, IoN will diminish and go into the locale underneath Curve 1, which is appeared as the shadow district in Fig. 4.

ISSN No: 2348-4845
International Journal & Magazine of Engineering, Technology, Management and Research
A Peer Reviewed Open Access International Journal

As of now, there is vitality bolstered back to the info. The vitality encouraged back achieves its biggest worth at most extreme info voltage and no heap, and for this situation, the pinnacle current of iLr equivalents to Vin m a x/Zr as appeared in Fig. 6. Keeping in mind the end goal to decrease the vitality nourished back at most extreme information voltage and noload, the trademark impedance of the thunderous tank, Zr , ought to be intended to be bigger. From Fig. 4, it can be watched that on Curve 1, when λ expands, IoN will increment. Since IoN=Iom a xZr/(nVin m in),Zris around proportionaltoIoN . That implies if λ is planned bigger, Zr can be intended to be bigger. In any case, if λ is intended to be bigger than the worth at point A, the converter will get into Mode 3 and the productivity will be debased. In this manner, λ and IoN at least information voltage and full load current are chosen at point An is the ideal decision.

2) Determine f_{sN} and V_{oN} :

As talked about above, λ and IoN at minimum information voltage and full load current ought to be planned at point A to minimize the vitality bolstered back to the information voltage, and in this manner to enhance the converter productivity. To encourage enhance the converter productivity, the time interim while iLr = 0 ought to be lessened, which relates to the time interim from t3 to Ts/2, as appeared in Fig. 5, since amid this time interim, the input voltage does not give vitality to the resounding tank. So it is best to diminish this time interim to zero, and hence, the converter works in basic CCM at least information voltage and full load current. At the point when the information voltage increments or burden current abatements, the converter will go into DCM. Along these lines, fs Nat least info voltage and full load ought to be designed as fsN = π/(α1 + α12 + α23), so that the converter works incritical CCM. Whenever λ, IoN and fsN are all decided, VoN can be controlled by (6).

TABLE II: FOUR SETS OF CONVERTER PARAMETER

Point	λ	I_{oN}	V_{oN}	f_{sN}
A_0	0	1	0.93	0.47
A_1	0.1	1.4	0.91	0.5
A	**0.217**	**2.2**	**0.8**	**0.52**
B	0.25	1.6	0.65	0.42

B. Compare the Set of Parameters at Point A with Other Three Sets of Parameters

To check that the point An is the ideal configuration point for λ and IoNat least information voltage and full load present, three otherpointsA0, A1, and B in Fig. 4, are decided for examinations. A0and A1are additionally on Curve 1. A0is a unique case as λ = 0,meaningCs is large to the point that it goes about as a dc piece capacitor and the converter really executes as a parallel full converter. A1is a point between A0andA.PointBcorresponds to theparameters that composed by [24], which is far from Curve 1.

Table II gives the relating λ, IoN ,VoN , and fsN of the centers A0 , A1 , An, and B at any rate data voltage and full load.Several segment burdens of these four focuses A0 ,A1 , An, and B are chosen for examinations, which include: 1) the rms estimation of iLr, meant by ILrrms , which can mirror the vitality criticism of the thunderous tank; 2) the pinnacle estimation of iLr, meant by ILrpk, which can mirror the pinnacle current of the force switches; 3) the pinnacle voltage of Cp, meant by V Cppk, which can mirror the pinnacle voltage of the rectifier diodes. To encourage computations, ILrrms,ILrpkare standardized concerning Io maxVo/Vin min, and VCppkis standardized as for Vo, and they are communicated as

$$\begin{cases} I^*_{L_r\_\mathrm{rms}} = \dfrac{I_{L_r\_\mathrm{rms}}}{I_{o\_\max} V_o / V_{\mathrm{in}\_\min}} = \dfrac{I_{L_r\mathrm{N}\_\mathrm{rms}}}{V_{oN} I_{oN}} \\ I^*_{Lr\_\mathrm{pk}} = \dfrac{I_{Lr\_\mathrm{pk}}}{I_{o\_\max} V_o / V_{\mathrm{in}\_\min}} = \dfrac{I_{L_r\mathrm{N}\_\mathrm{pk}}}{V_{oN} I_{oN}} \\ V^*_{C_p\_\mathrm{pk}} = \dfrac{V'_{C_p\_\mathrm{pk}}}{V_o} = \dfrac{V_{C_p\mathrm{N}\_\mathrm{pk}}}{V_{oN}}. \end{cases} \quad (11)$$

$$\begin{cases} n = \dfrac{V_{oN} V_{\mathrm{in}\_\min}}{V_o} \\ L_r = \dfrac{n V_{\mathrm{in}\_\min} I_{oN} f_{sN}}{2\pi f_{s\_\max} I_{o\_\max}} \\ C'_p = \dfrac{n(1+\lambda) I_{o\_\max} f_{sN}}{8\pi f_{s\_\max} V_{\mathrm{in}\_\min} I_{oN}} \\ C_s = \dfrac{(1+\lambda) I_{o\_\max} f_{sN}}{2\pi\lambda f_{s\_\max} n V_{\mathrm{in}\_\min} I_{oN}}. \end{cases} \quad (12)$$

ISSN No: 2348-4845
International Journal & Magazine of Engineering, Technology, Management and Research
A Peer Reviewed Open Access International Journal

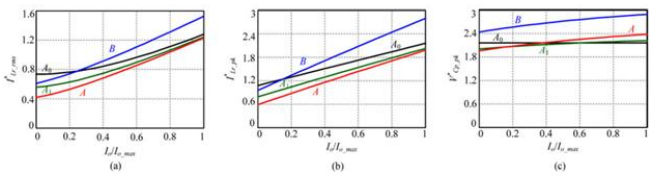

Fig 7: Component Stresses at different load under minimum input voltage

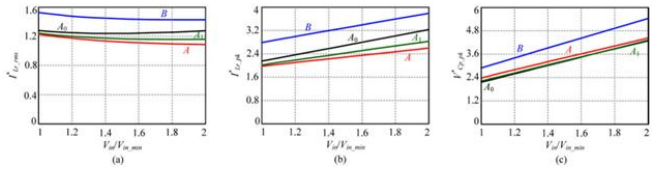

Fig 8: Component Stresses at different full load under minimum input voltage

According to (6), (8), (9), and (10), I∗Lrrms, I∗Lrpk, and V ∗Cppk in (11) can be obtained when λ, IoN, and fsN are given. The curves of I∗Lrrms, I∗Lrpk, and V ∗Cppk at different load and input voltage are depicted in Figs. 7 and 8. According to Figs.7 (a) and 8(a), I∗Lrrms at A is the smallest among A0, A1, A, and B when input voltage and load current changes. According toFigs. 7(b) and 8(b), I∗Lrpk at A is also the smallest. According to Figs. 7(c) and 8(c), the maximum value of V ∗Cppk in the variation ranges of input voltage and load current at point A is a littlehigher than that at A0 and A1, but lower than that at B. SinceI∗Lrrms plays a more important role for conduction losses, the point A corresponds to the optimal converter parameters. Therefore, these curves in Figs. 7 and 8 have verified the parameter sat the point A are optimal.

D. Design Procedure

1) Determine the Normalized Parameters According to the Point A with a Certain Margin:

While applying the set of parameters of the point A in Table II, a certain margin should be kept to prevent the converter from entering non-ZCS area, Mode 3, or CCM. This means λ, I_{oN}, V_{oN}, and f_{sN} should be a little smaller than that at point A. When the detailed converter specification, which includes the minimum input voltage V_{inmin}, the full load current I_{omax}, the output voltage V_o , and the maximum switching frequency $f_{smax}$are given, λ, I_{oN}, V_{oN}, andf_{sN}can be converted into the real converter parameters as Three prototypes of DCM LCC resonant converter with inductive filter have been designed with the same specification, where V_{inmin}= 500V,V_{inmax}= 600V, V_O= 50V,I_{omax}= 100 parameters at point A. From Table II, to keep a certain margin, we choose λ = 0.21, IoN = 1.7, VoN = 0.7, and fsN = 0.44. Prototype 2 and prototype 3 are designed with the set of parameters at point B and point A0 for comparison with the prototype 1. For prototype 2, λ = 0.25, IoN = 1.6, VoN = 0.6, and fsN = 0.38 are chosen to keep a certain margin. For prototype 3, λ = 0.01, IoN = 0.8, VoN = 0.8, and fsN = 0.42 are chosen to keep a certain margin. From (12), the real converter parameters of these three prototypes are obtained as shown in Table III. For a fair comparison, these three

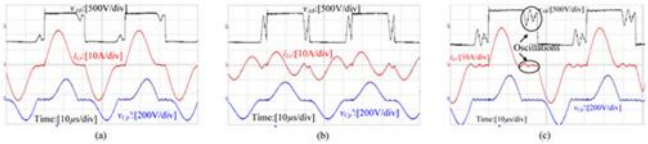

Fig. 9. Experimental waveforms in prototype 1. (a) V_{in} = 500 V, I_o = 100 A. (b) V_{in} = 500 V, I_o = 10 A. (c) V_{in} = 600 V, I_o = 100 A.

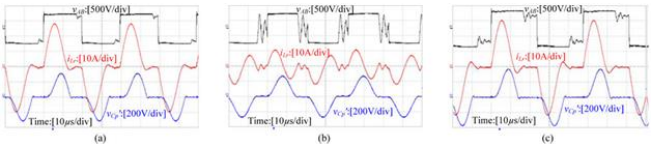

Fig. 10. Experimental waveforms in prototype 2. (a) V_{in} = 500 V, I_o = 100 A. (b) V_{in} = 500 V, I_o = 10 A. (c) V_{in} = 600 V, I_o = 100 A.

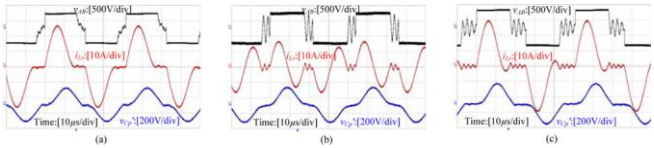

Fig. 11. Experimental waveforms in prototype 3. (a) V_{in} = 500 V, I_o = 100 A. (b) V_{in} = 500 V, I_o = 10 A. (c) V_{in} = 600 V, I_o = 100 A.

Prototypes adopt the same IGBTs (FF50R12RT4 from Infineon), rectifier diodes (DSEI2×101-06A from IXYS), Lf and Cf, where Lf = 40Mh and Cf= 3760 μF.

ISSN No: 2348-4845
International Journal & Magazine of Engineering, Technology, Management and Research
A Peer Reviewed Open Access International Journal

TABLE III: PARAMETERS OF THE THREE PROTOTYPES

	L_r	C_r	C_p'	n:1:1
Prototype 1	180 μH	0.30 μF	0.76 μF	7:1:1
Prototype 2	125 μH	0.27 μF	0.60 μF	6:1:1
Prototype 3	90 μH	10 μF	1.5 μF	8:1:1

Figs. 9–11 show the experimental waveforms of the three prototypes at different input voltage and load. From the three figures, the following can be seen:

1) The IGBTs in all the three prototypes all achieve ZCS at different input voltage and load.
2) As seen in Fig. 9(c), parasitic oscillations appear in vABand iLr. This is caused by the resonance of Lrand the junction capacitors of IGBTs when all the IGBTs are turned off. The energy stored in the junction capacitors of IGBTs is dissipated in the course of the oscillations, which will reduce the converter efficiency. Therefore, it is better to choose the IGBTs, which have small junction capacitors.
3) As seen in Figs. 9(a), 10, (a) and 11(a), when V_{in} = 500 V and I_o = 100 A, prototype 1 and prototype 3 operate near the boundary of Mode 1 and non-ZCS area, and prototype 2 operates in Mode 2. As seen in Figs. 9(c), 10(c), and 11(c), when V_{in} = 600 V and I_o = 100 A, prototype 1 and prototype 2 operate in Mode 2, and prototype 3 operates in Mode 1. They are well in agreement with the mode boundary map.
4) The peak value of i_{Lr} in prototype 1 is smaller than that in prototype 2 and prototype 3 with the variations of input voltages and loads. That indicates that prototype 1 can achieve a higher efficiency over the entire input voltage and load range.

Fig. 12(a) shows the measured efficiencies of these three prototypes versus load currents when V_{in} = 500 V. Fig. 12(b) shows the measured efficiency of these three prototypes versus input voltages when I_o = 100 A. It can be seen that the efficiency of prototype 1 is higher than prototype 2 and prototype 3. It has verified that the set of parameters near point A is optimal.

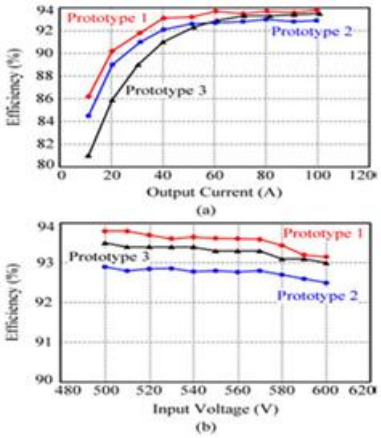

Fig. 12. Efficiency curves (a) versus load at minimum input voltage (V_{in} = 500 V) and (b) versus input voltage at full load (I_o = 100 A).

Fig. 13(a) demonstrates the deliberate exchanging frequencies of these three models versus load streams when Vin = 500 V. It can be seen that in any of these three models, the recurrence keeps about unaltered when the heap changes, which confirms the DCM LCC resounding converter has a well steady yield voltage trademark. Fig. 13(b) demonstrates the deliberate exchanging frequencies of these three models versus information voltages when Io = 100 A. As seen, in any of these three models, the exchanging recurrence is directly decreased with the expansion of information voltage, which is very much fulfilled by (7).

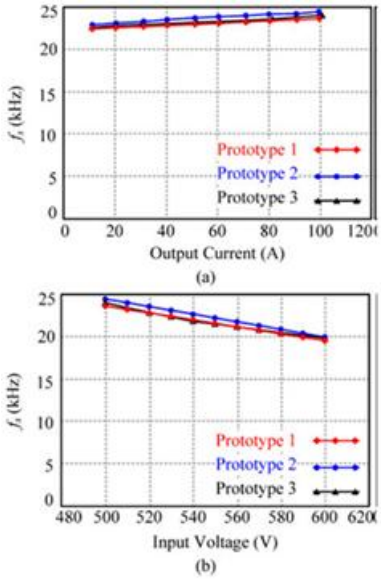

ISSN No: 2348-4845
International Journal & Magazine of Engineering, Technology, Management and Research
A Peer Reviewed Open Access International Journal

Fig. 13. Switching frequency curves (a) versus load at minimum input voltage (V_{in} = 500 V) and (b) versus input voltage at full load (I_o = 100 A).

VII. CONCLUSION:

Three fundamental working methods of DCM LCC thunderous converter with inductive channel have been audited. With a specific end goal to decide the parameter scope of each working mode, the mode limit guide of the converter has been inferred. Based the mode limit outline, set of ideal and standardized parameters has been found by a summed up ideal configuration. A few different arrangements of parameters are contrasted and the arrangement of ideal parameters by different outline bends. Since this arrangement of parameters is standardized, it can be changed over into genuine parameters as indicated by the converter particular. Tests have checked that with this arrangement of parameters, the converter has a high proficiency over the whole information voltage and burden range.

REFERENCES:

[1] L. Sun, J. He, Y. Pei, and Z. Wang, "Design and optimization of high current intelligent waveform power supply for electroplating," in Proc.IEEE Power Electron. Motion Control Conf., 2012, pp. 1516–1521.

[2] I. D. Kim, W. W. Cho, J. Y. Kim, and E. C. Nho, "Design of low-voltage high-current rectifier with high-efficiency output side for electrolytic dis-infection of ballast water," in Proc. IEEE Energy Convers. Congr. Expo., 2010, pp. 1652–1657.

[3] N. Frohleke, H. Mundinger, S. Beineke, P. Wallmeier, and H. Grotstollen, "Resonant transition switching welding power supply," in Proc. IEEE Ind.Electron., Control Instrum., 1997, pp. 615–620.

[4] E. J. Dede, G. Garcera, V. Esteve, J. M. Benavent, J. A. Carrasco, and A. Ferreres, "On the design of a high current power supply for super-conducting magnet," in Proc. IEEE Power Electron. Spec. Conf., 1996, pp. 894–897.

[5] G. Ivensky, I. Zeltser, A. Kats, and S. Ben-Yaakov, "Reducing IGBT losses in ZCS series resonant converters," IEEE Trans. Ind. Electron., vol. 46, no. 1, pp. 67–74, Feb. 1999.

[6] Y. Lo, C. Lin, M. Hsieh, and C. Lin, "Phase-shifted full-bridge series-resonant DC–DC converter for wide load variations," IEEE Trans. Ind.Electron., vol. 58, no. 6, pp. 2572–2575, Jun. 2011.

[7] H. Sheng, W. Shen, H. Wang, D. Fu, Y. Pei, X. Yang, F. Wang, D. Boroye-vich, F. C. Lee, and C. W. Tipton, "Design and implementation of a high power density three-level parallel resonant converter for capacitor charging pulsed-power supply," IEEE Trans. Plasma Sci., vol. 39, no. 4, pp. 1131–1140, Apr. 2011.

[8] R. L. Steigerwald, "A comparison of half-bridge resonant converter topologies," IEEE Trans. Power Electron., vol. 3, no. 2, pp. 174–182, Apr. 1988.

[9] R. P. Severns, "Topologies for three-element resonant converter," IEEETrans. Power Electron., vol. 7, no. 1, pp. 89–98, Jan. 1992.

[10] I. Batarseh, "Resonant converter topologies with three and four energy storage elements," IEEE Trans. Power Electron., vol. 9, no. 1, pp. 64–73, Jan. 1994.

[11] B. Yang, F. C. Lee, A. J. Zhang, and G. Huang, "LLC resonant converter for front end DC/DC conversion," in Proc. IEEE Appl. Power Electron.Conf. Expo., 2002, pp. 1108–1112.

[12] W. Feng and F. C. Lee, "Optimal trajectory control of LLC resonant converter for soft start-

up," IEEE Trans. Power Electron., vol. 29, no. 3, pp. 1461–1468, Mar. 2014.

[13] A. J. Gilbert, C. M. Bingham, D. A. Stone, and M. P. Foster, "Normalized analysis and design of LCC resonant converters," IEEE Trans. PowerElectron., vol. 22, no. 6, pp. 2386–2402, Nov. 2007.

[14] D. Fu, F. C. Lee, Q. Yang, and F. Wang, "A novel high-power-density three-level LCC resonant converter with constant-power-factor-control for charging applications," IEEE Trans. Power Electron., vol. 23, no. 5, pp. 2411–2420, Sep. 2008.

[15] J. Liu, L. Sheng, J. Shi, Z. Zhang, and X. He, "LCC resonant converter op-erating in discontinuous resonant current mode in high voltage, high power and high frequency applications," in Proc. IEEE Appl. Power Electron.Conf. Expo., 2009, pp. 1482–1486.

[16] J. Biela, U. Badstuebner, and J. W. Kolar, "Design of a 5-kW, 1-U, 10-kW/dm3 resonant DC–DC converter for telecom applica-tions," IEEE Trans. Power Electron., vol. 24, no. 7, pp. 1701–1710, Jul. 2009.

[17] T. Soeiro, J. Muhlethaler, J. Linner, P. Ranstad, and J. Kolar, "Auto-mated design of a high power high frequency LCC resonant converter for electrostatic precipitators," IEEE Trans. Ind. Electron., vol. 60, no. 11, pp. 4805–4819, Nov. 2013.

[18] G. Ivensky, A. Kats, and S. Ben-Yaakov, "An RC load model of paral-lel and series-parallel resonant DC–DC converters with capacitive out-put filter," IEEE Trans. Power Electron., vol. 14, no. 3, pp. 515–521, May 1999.

[19] R. Yang, H. Ding, Y. Xu, L. Yao, and Y. Xiang, "An analytical steady-state model of LCC type series-parallel resonant converter with capacitive output filter," IEEE Trans. Power Electron., vol. 29, no. 1, pp. 328–338, Jan. 2014.

[20] A. J. Forsyth, G. A. Ward, and S. V. Mollov, "Extended fundamental frequency analysis of the LCC resonant converter," IEEE Trans. PowerElectron., vol. 18, no. 6, pp. 1286–1292, Nov. 2003.

[21] A. K. S. Bhat, "Analysis and design of a series–parallel resonant con-verter," IEEE Trans. Power Electron., vol. 8, no. 1, pp. 1–11, Jan. 1993.

[22] A. K. S. Bhat, "Analysis and design of a high-frequency resonant con-verter using LCC-type commutation," IEEE Trans. Power Electron., vol. 2, no. 4, pp. 291–301, Oct. 1987.

[23] S. Shah and A. K. Upadhyay, "Analysis and design of a half-bridge series-parallel resonant converter operating in discontinuous conduc-tion mode," in Proc. IEEE Appl. Power Electron. Conf. Expo., 1990, pp. 165–174.

[24] V. Belaguli and A. K. S. Bhat, "Series-parallel resonant converter operating in discontinuous current mode-analysis, design, simulation, and experi-mental results," IEEE Trans. Circuits Syst., vol. 47, no. 4, pp. 433–442, Apr. 2000.